Vessel-based lung lobe partitioning in ultra-short time echo proton MRI for regional ventilation assessment

Rezkellah Noureddine Khiati, Antoine Didier, Nathalie Barrau, Aurelien Justet, Xavier Maître, Jean-François Bernaudin, Pierre-Yves Brillet, Ruxandra Tapu, Radu Ispas, Catalin Fetita

Vessel-based lung lobe partitioning in ultra-short time echo proton MRI for regional ventilation assessment

Rezkellah-Noureddine Khiati[1,7*], Antoine Didier[1], Nathalie Barrau[2], Aurélien Justet[3], Xavier Maître[2], Jean-François Bernaudin [4,5,6], Pierre-Yves Brillet[4,5], Ruxandra Tapu[1], Radu Ispas[7] and Catalin Fetita[1*]

[1] *SAMOVAR, Telecom Sud-Paris, Institut Polytechnique de Paris, Evry, France*

[2] *Université Paris-Saclay, CEA, CNRS, Inserm, BioMaps, Orsay, France*

[3] *Pneumologie & Médecine Nucléaire CHU Caen, France*

[4]*Avicenne Hospital, AP-HP, Bobigny, France*

[5]*INSERM 1272 Université Sorbonne Paris Nord, Bobigny, France*

[6] *Sorbonne Université Paris*

[7] *Keyrus France, Levallois-Perret, France*

*these authors have contributed equally

Abstract.

This paper addresses the problem of lung lobe partitioning in ultra-short time echo (UTE) MRI acquisitions, which are recently used for lung ventilation assessment with MRI spirometry. Because of the low image contrast, which does not enable the lung fissures display, the developed approach relies only on the vascular structures which still can be segmented from these images. The vascular network is segmented in lobes in order to generate reference clusters used for lung space partitioning. A point cloud representing the unstructured points of the vascular medial axis is partitioned in five lobes exploiting the PointNet++ framework. The PointNet++ model is trained on data extracted from CT acquisitions and labeled using the airway and vascular trees connectivity. The airway tree lobes will define the lung lobar regions, which are propagated on the vessel structure to achieve the complete vascular labeling. A separate model is trained for the right and left lungs in order to alleviate for limited input point cloud size imposed by the model architecture and reach a high precision in classification. The trained model is applied to UTE-MRI data to generate, for a given subject, a point cloud reference that will be used for vascular lobes clustering, which will be then exploited for lung space partitioning in lobes. The approach was quantitatively evaluated on 10 CT volumes from LUNA16 dataset and qualitatively tested on additional 25 CT and 15 UTE-MRI datasets. The analysis of CT data results shows pertinent lung partitioning with respect to the lung fissures, even if a precise fissure localization is not achieved. Such result is however expected, since no information related to the lung fissure is exploited in our method because this would not be applicable to UTE-MRI data. Nevertheless, the proposed partitioning respects the vascular lobes and, to the best of our knowledge, is novel for lung MRI sequences making it possible the regional investigation of ventilation parameters in MRI spirometry. The method can be further on extended for lung fissure matching in CT data by integrating new constraints related to fissure detection.

Keywords: ultra-short time echo MRI, lung lobe segmentation, computed tomography, point cloud, clustering, pulmonary vascular segmentation

1. Introduction

Lung lobe partitioning in pulmonary image analysis is required whenever regional investigation at lobar level is aimed. While CT remains the current imaging modality for lung assessment because of its high contrast in depicting textural patterns, proton MRI has shown increasing potential for studying lung ventilation mapping [1, 2], with ultra-short time echo (UTE) acquisitions approaching images obtained in CT [3]. Note however that, when lung disease is present (in particular, ground glass and fibrosis patterns) or in case of low contrast images, lung fissures are not distinguishable even on CT images (Fig. 1) and classic approaches used for lung lobe segmentation [4-10] would fail. UTE-MRI images exhibit

lower contrast than CT ones, missing the lung fissure even for healthy subjects.

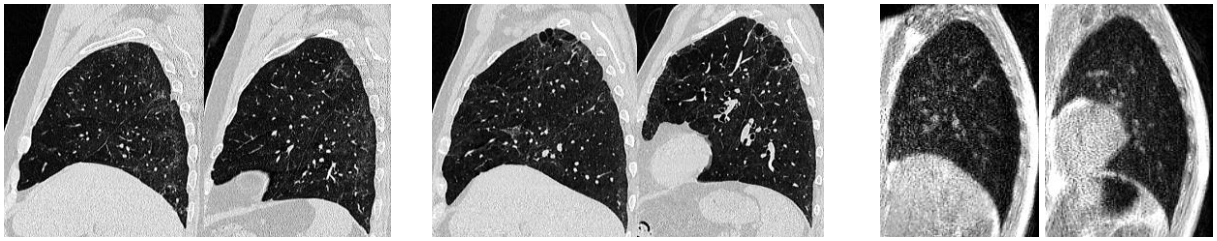

(a) CT - COVID follow-up subject (b) CT - COVID follow-up subject (c) UTE-MRI – healthy subject

Figure 1. Examples of CT and UTE-MRI sagittal images (right/left lungs) with increasing difficulty for lung fissure depiction (from left to right) due to pathology or low contrast data.

The objective of this paper is to develop a method able to provide lobar partitioning of lungs in UTE-MRI (as well as in low-contrast CT) without relying on the lung fissure detection. In this respect, we intend to exploit the pulmonary vessel segmentation and the lobe clustering of the vascular tree to infer the lung partitioning into lobes. The advantages and limitations of the proposed approach will be discussed with respect to state-of-the-art while keeping in mind that our objective is not an accurate lung fissure detection (which will not be possible in UTE-MRI).

2. Materials and methods

CT and UTE-MRI images provide enough contrast for lungs and intra-pulmonary vessels segmentation, with lung fissures location relatively well-distinguishable on vessel medial axis (Fig. 2), which suggests the possibility of vessel tree partitioning according to lung lobes. When achieved, such partitioning may define the lung separation in lobes. The key point is how obtaining the vessel tree clustering into five lobes knowing that vessel connections between lobes may occur mostly due to pathology presence, inducing segmentation errors. A possible solution for CT images would rely on airway tree segmentation and partitioning in lobar segments; because of the spatial proximity between airway and vascular trees, airway lobar segments may identify their counterpart in the vascular tree. Eventual connections between vascular lobes can be detected when points of different airway lobes would lead to the same vessel lobe; such connections will be removed using graph cut and the vascular tree will be labeled according to the lung lobes (Fig.3). Note however that such strategy cannot be applied for UTE-MRI data because the low image contrast makes impossible the airway tree segmentation to a sufficient subdivision level to be exploited in vessel tree labeling. In view of this limitation, we propose a hybrid machine learning approach to perform the lobes identification of the vessel tree, by considering the vessel axis points as an unstructured point cloud and use the PointNet++ framework [11] to achieve the lobe clustering. The vessels medial axis will be thus labeled based on the point clusters (with graph cuts applied to lobe connections when necessary) and the lung partitioning in lobes is finally achieved based on the labeled vessels.

In order to infer the vessel point cloud clustering, PointNet++ is trained on data generated from CT acquisitions by applying the vessel lobes identification using airway tree segments. The complete method is detailed in the following.

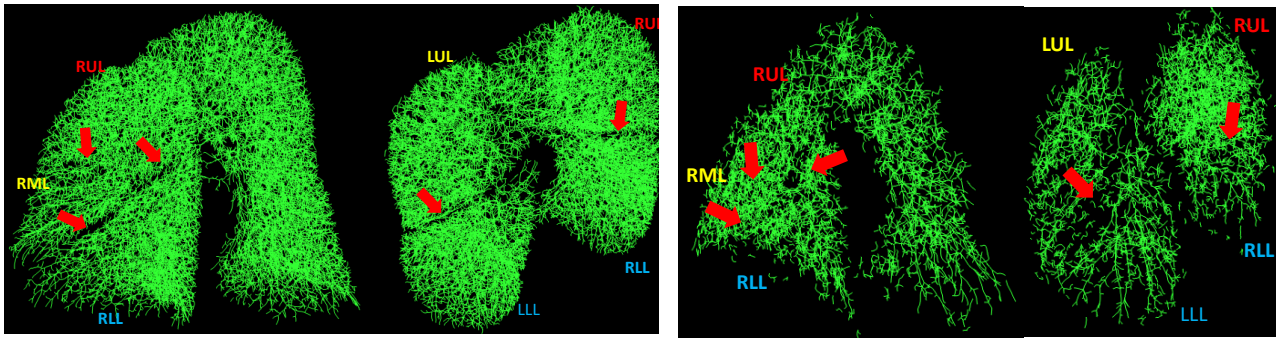

(a) vessel segmentation from CT (b) vessel segmentation from UTE-MRI

Figure 2. Medial axis of vascular tree showing lung fissure location – red arrows (lateral anterior and lateral posterior views). RUL-right upper lobe, RML-right middle lobe, RLL-right lower lobe, LUL-left upper lobe, LLL- left lower lobe.

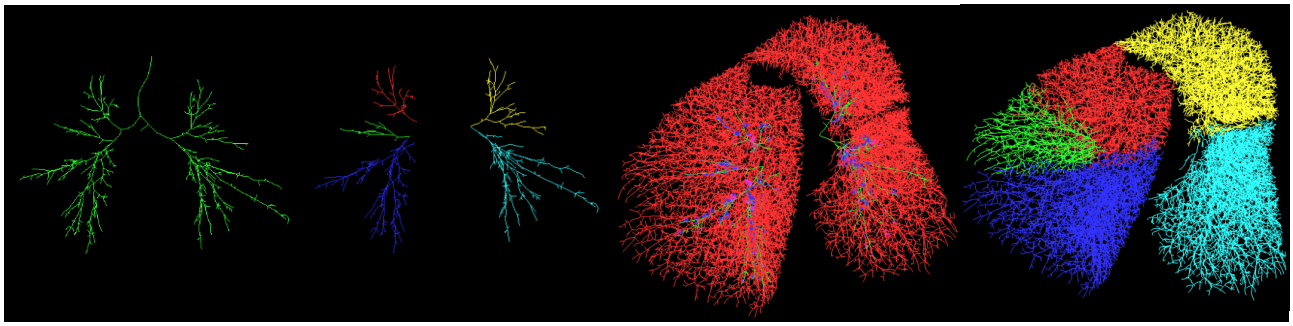

(a) airway medial axis (b) airway lobar segments [12] (c) airway (green)-vessel (red) pairing (blue) (d) vessel lobar partitioning

Figure 3. Vessel tree labeling based on airways.

2.1. Point cloud data generation for training vessel clustering in lobes

For both CT and UTE-MRI data, lung and vessels segmentation is performed using the generic approaches of [13] and [14, 15], respectively. The medial axis of vascular structures is extracted according to [16], each axis point containing the vessel caliber information. In order to build-up a training database for vascular clustering, we selected 40/5/25 CT data acquisitions from a COVID follow-up database in Caen University Hospital, France (COVALung study) as train/validation/test sets respectively. For these datasets, airway tree segmentation was performed [17] followed by medial axis computation [16] and airway lobes detection [12] (Fig. 3a,b).

Because the airway segments follows closely the pulmonary arteries (similar direction and calibers), the joint analysis of labeled airway and vascular trees allows identifying airway-vessel pair points [18] (Fig. 3c) and assigning the lobar labels to vascular segments. These labels are propagated to the segment root and, in the eventuality of different labels assigned to the same root (induced by lobes interconnection on the vascular graph), a graph cut removes the connection between lobes to ensure a unique label for each vessel subtree. The cut point on the path linking two lobes is set at half angle between the corresponding airway lobar segments. The result of vessel lobe partitioning is shown in Fig. 3d. From this result, we generate the associated point cloud as input training data together with point labels as target classes. Note that a separate subset is generated for each lung with 3 and 2 classes as target for the right and left lungs respectively, and two models are trained for each lung clustering (Fig. 4). The vessel points ground truth labeling may however include some misclassification errors near the fissures since the graph cut criterion does not guarantee sufficient robustness. These errors may affect the classification output and will be taken into account in the lung lobe partitioning procedure.

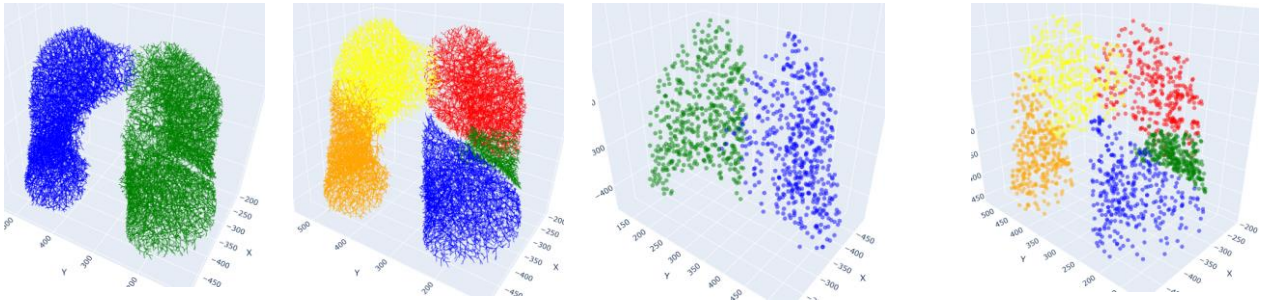

(a) input point cloud (b) associated point labels (c) uniform sample of (a) of 1024 points (d) associated labels of (c)

Figure 4. Example of point cloud input data for PointNet++ based classification.

2.2. Lung point cloud clustering using PointNet++

PointNet++ [11] is a model dedicated to point cloud segmentation and uses a hierarchical neural architecture. It partitions the point cloud into overlapping local regions by sampling and grouping points in a manner similar to the traditional convolution operation, which enables capturing features at various scales.

Not that the original PointNet model is able to recognize global structures but struggles with capturing the intricate, local geometric structures, particularly when these structures vary in scale. PointNet treats each point independently and does not effectively capture the relationships between points in local neighborhoods. PointNet++ addresses this issue by hierarchically sampling and grouping points to capture fine geometric structures. For each local region, a mini-PointNet is used to extract features from points in that region. These features are then used by subsequent layers or for the final task (classification or segmentation).

2.2.1. Sample size and selection

The lung lobe point clouds from our training dataset consist of variable number of points, larger than the model input requirements. To ensure consistent data input for our model, the input batch size needs to be standardized in a manner ensuring a fixed number of points from each patient dataset. In this respect, we adopted a stratified sampling technique to curate point cloud batches, each comprising 1024 points. Given their anatomical distinction, we processed individually the right and the left lungs, and built a separate model for each lung clustering.

For the right lung, the target classes represent upper lobe, middle lobe, and lower lobe, respectively. For standardization, we sampled 341 points from each class, totaling 1023 points. An additional point was sourced from the middle lobe, which is notably underrepresented in our test dataset, bringing the aggregate to 1024 points per batch. This sampling procedure was reiterated until a class was depleted of sufficient points for the aforementioned stratification.

For the left lung, however, our stratified approach was slightly adjusted. The left lung encompasses two classes, upper lobe and lower lobe. We uniformly sampled 512 points from each of these classes to compile the batch of 1024 points.

The sampling strategy can be summarized as follows. Let P denotes a single point cloud dataset and $n_{batches}$ denote the number of batches derived from each patient dataset.

Each batch comprises 1024 points, and each point has three coordinates (X, Y, Z).Therefore, the dimensions of the data for each patient can be described as:

$$P = n_{batches} * 1024 * 3. \quad (1)$$

Given the sampling strategy for the right lung:

$$nC_1 = nC_2 = nC_3 = 341\,. \quad (2)$$

nC_2 is incremented by 1 for a total of 342 for each batch.

$$Batch_{right} = nC_1 + nC_2 + nC_3 = 341 + 342 + 341 = 1024. \quad (3)$$

The iterative process for the stratified sampling continues until at least one class cannot provide the required point number:

$$Repeat\ until \min(nC_1, nC_2, nC_3) < 341\,, \quad (4)$$

where $\min(nC_1, nC_2, nC_3)$ represents the smallest count among the three classes. The same strategy is applied to the left lung, but with nC_4 and nC_5 equal to 512.

Upon completion, each patient dataset will have been transformed into a series of batches, each of size 1024*3, and the total number of batches is n_{batches}.

2.2.2. Data preprocessing

For each batch of point cloud data comprising 1024 points, a normalization of the spatial coordinates was performed using the z-score method. Mathematically, for each point p_i in a batch, its standardized version p_i' is computed as:

$$p_i' = \frac{p_i - \mu_p}{\sigma_p} \quad (5)$$

2.2.3. Calculation of point normals

For enhanced feature representation and subsequent processing of our point cloud data, normals were computed for each point. Normals, in the context of point clouds, represent vectors that are perpendicular to the tangent plane at a given point. These vectors can provide valuable information about the local geometric structure, aiding in tasks such as segmentation, registration, and feature extraction.

Upon calculating the normals for each point in the point cloud, these were appended as additional channels to the input data for the model. Originally, the model processed point cloud data using only 3 channels corresponding to the (x, y, z) coordinates. With the inclusion of the normals, the input channels increased to 6: the original (x, y, z) coordinates and the three components of the corresponding normals. This enriched the representation, by combining both positional and local geometric structure information.

2.2.4. Training

We trained two distinct models, each dedicated to either the right or left lung. Both models share identical hyperparameters. The Cross Entropy loss function, combined with a Softmax activation, was used for training. The Adam optimizer was employed with a learning rate of 10^{-3}, and the training persisted for 100 epochs.

2.2.5. Model performance on validation set

The two models demonstrated commendable robustness and generalizability when evaluated on the validation dataset, despite its limited size in terms of the number of patients. Specifically, for the left lung, the model achieved an accuracy of 95%. Remarkably, the performance was even superior for the right lung, with the model registering an accuracy of 98%. These results underscore the efficacy of the two models, emphasizing their capabilities to deliver high predictive accuracy. As illustrated in the figures below (Fig. 5), it is obvious that our model exhibits a slight tendency towards overfitting. This is primarily attributed to the limited number of samples in our training dataset.

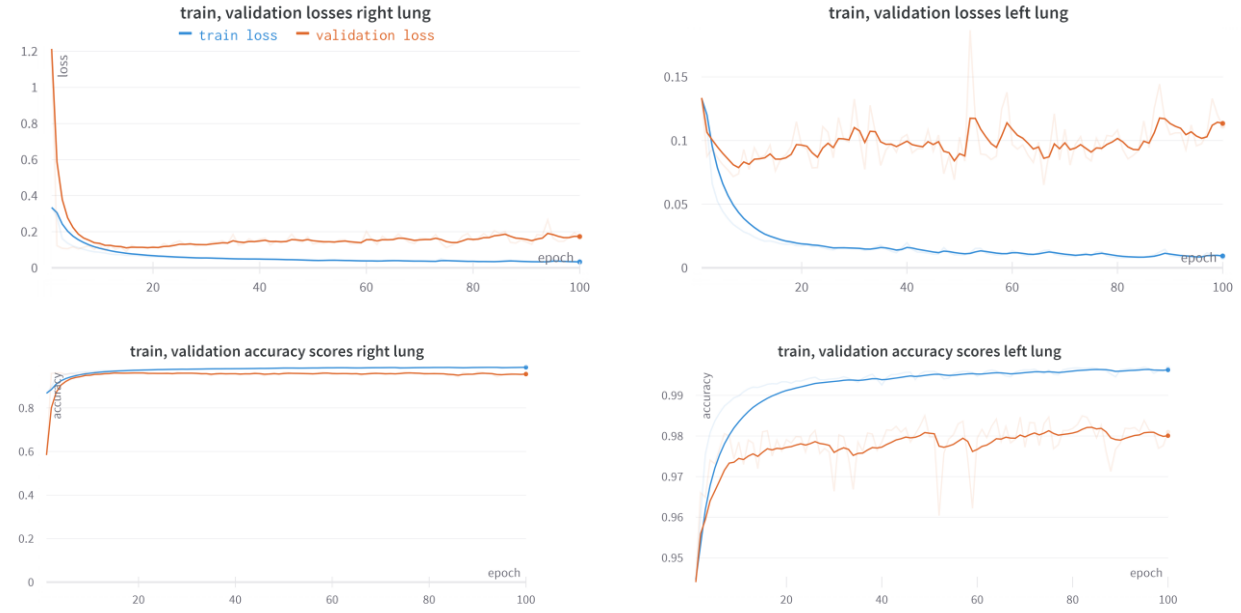

Figure 5. Train and validation losses and accuracies for the two models PointNet++ for the right and the left lungs.

2.3. Lobes segmentation on CT and UTE-MRI data

Lung lobe partitioning based on the vascular clustering on a test dataset operates as follows. First, the segmentation of lungs and vessels is achieved (Fig. 6a) followed by vascular point cloud clustering using the PointNet++ models (Fig. 6b,

§2.2). In order to alleviate for point cloud classification errors near the fissures, points with neighbors of different label in a 6x6x6 mm^3 ROI are filtered out. In addition, from each point cloud cluster, a compact subset is built-up to define the space region associated with its label (Fig. 6c). The resulting labeled point cloud is then used to perform the vessel axis labeling instead of using the airway tree lobar segments as done for point cloud training set generation (the segmented airway tree being unavailable for UTE-MRI data). In our experiments, in order to reduce the probability of lobes interconnection on the vessel medial axis, terminal segments of vessels with caliber less than 1.5 mm radius were removed from the vessel axis, leading to a less dense axis. To avoid redundant computation for axis labeling, we exploited only the points in the labeled point cloud corresponding to the terminal points of the vessel axis. In case of graph cut, the cutting point on the path linking two lobes is chosen in the space area separating the labels in Fig. 6c by maximizing the distance to these labels. The labeled vessel axis tree is shown in Fig. 6d (corresponding to the less dense version of the axis).

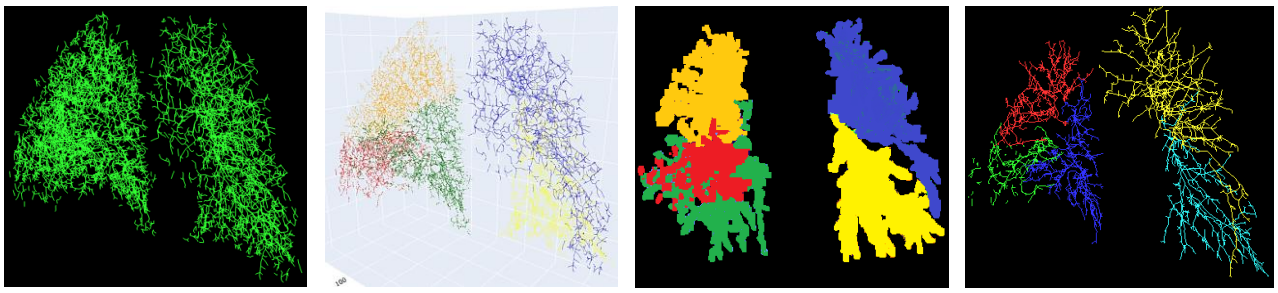

(a) initial vessel axis (b) point cloud clustering (c) compact cluster regions (d) vessel axis partitioning

Figure 6. Synopsis of the vessel axis partitioning based on point cloud clustering (UTE-MRI data).

Based on the labeled vessel axis, each labeled region will generate a compact subset using morphological closing with a large spherical structuring element (20-voxel size radius) followed by a small erosion in order to ensure spacing between the lobe labels (Fig. 7a). A space partitioning between the compact subsets, based on Euclidean distance, will provide the lung separation into lobar regions. A final regularization ensures the smoothing of the lobe surfaces by assigning in each point the maximum occurrence label in a 11^3 voxels neighborhood (Fig. 7b-d).

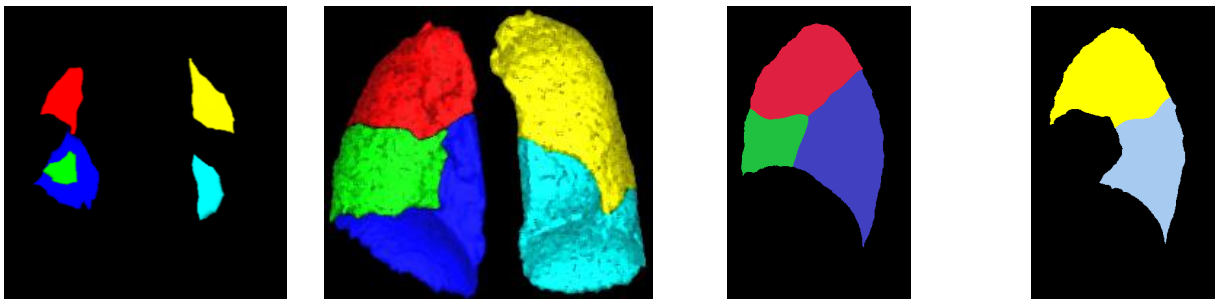

(a) vessel axis (compact) clusters – frontal view (b) lobe partitioning of lung based on (a) (c) sagittal view right lung, of Fig. 1c (d) sagittal view left lung, of Fig. 1c

Figure 7. Lung lobes partitioning based on vessel axis lobes.

3. Results and discussion

The proposed approach was first evaluated on CT data, since the fissure location is only visible on CT. A first qualitative investigation was conducted to check if the lung partitioning in lobes could also be achieved directly from the vessel point cloud clustering (Fig. 6b,c) instead of vessel axis partitioning (Fig. 6d). The qualitative test dataset included 25 CT scans not used in the PointNet++ training, from a retrospective COVID follow-up cohort collected at Caen University Hospital,

France. The visual investigation showed that the lobe partitioning based solely on point cloud clustering presents generally an overestimation of the right middle lobe, while similar performance is achieved for the left lobes (Fig. 8). This is explained by the fact that vessel axis partitioning based on point cloud clustering can correct some prediction errors near the fissures.
As can be seen in Fig. 8 top, the lobes identification in the CT images is pertinent with respect to the fissure locations. However, the fissure is not accurately localized. This limitation can be explained by the fact that no information regarding the fissure is taken into account, because such information is not available in UTE-MRI data.

We conducted a second quantitative investigation on a subset of publicly available CT data including lung lobes segmentation ground truth. In order to assess the performance of our model against available methods, we randomly selected 10 patients from the LUNA16 dataset, which consists of 50 CT annotated patients representing the lung lobes. To the best of our knowledge, this annotated CT dataset is the only publicly available, and no MRI annotated data for lung lobes was found. Since this dataset is distinct from our training and validation sets, we first preprocessed the data by resizing the spacing to achieve isotropic dimensions of 0.6 mm per pixel in each axis (x, y, z). A grayscale windowing was applied in the interval [-1000, -600] HU. The lung segmentation procedure discussed in §2 was applied and the results were assessed in comparison with the method in [4] evaluated on the same database, Table 1.

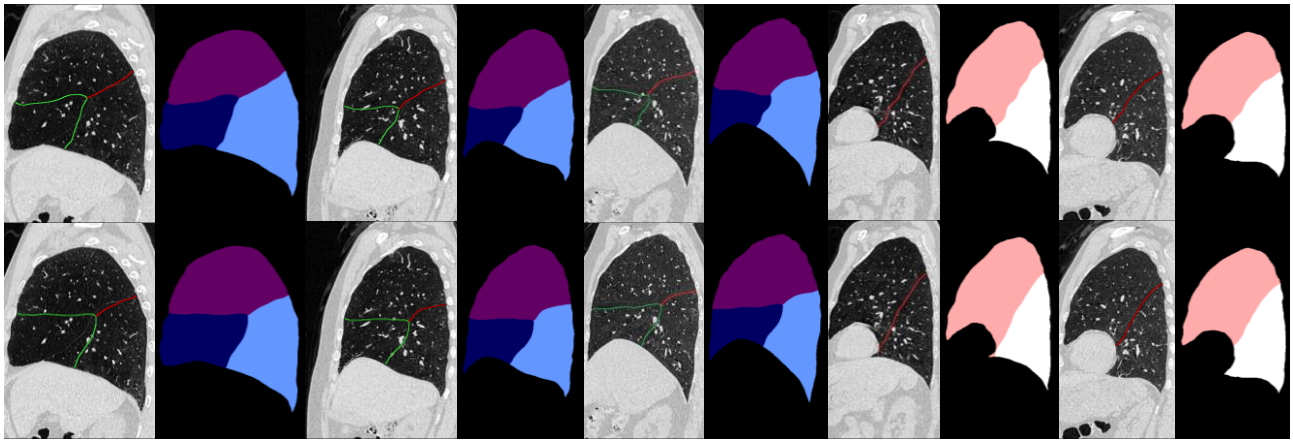

Figure 8. Comparison of lobe partitioning result (CT images) between the proposed approach using vessel axis partitioning (top) and the alternative using direct point cloud clustering (bottom). Lobes interface is shown in color on original sagittal images for comparison with the real fissure location.

Dice scores achieved on LUNA16 test set

	Right lung			Left lung		
	RU	RM	RL	LU	LL	AVG
[4]	92.53	80.60	93.05	96.10	95.30	91.48
proposed method	91.07	80.30	90.71	95.44	94.35	90.37

Table 1: Comparative Analysis of Dice scores between the proposed and the method in [4]. RU, RM, RL, LU, LL and AVG represent Dice coefficients of right upper lobe, right middle lobe, right lower lobe, left upper lobe, left lower lobe and their average, respectively.

As shown in Table 1, the segmentation results obtained by our method are very close to the performance of the reference method. Note that the test sets might not be exactly the same for the compared methods, given their random selection in [4] and in our method. However, since our method is trained on a completely different dataset outside LUNA16 database, the results obtained demonstrate the robustness and the generalization capability of our method.

Figure 9 depicts few representative examples of lobe segmentation obtained with the proposed method, compared versus the ground truth masks, with fissure locations delineated on the original grayscale sagittal images. We can note the results across various lobes of the lungs were promising, with lower accuracy achieved for the segmentation of the right middle lobe, which continues to pose a significant challenge. An explanation may come from the small size of the RML vascular tree, more prone for labelling errors. The state-of-the-art methods such [4] encounter the same difficulty since in a large number of cases, the fissures separating the right middle and lower/upper lobes are not distinctly visible or are only partially seen in images. A potential improvement of the proposed approach for lobe segmentation from CT data would be to detect and take into account the fissure information and to warp the actual results to the fissures, but such work is beyond the scope of this paper.

A second qualitative investigation was performed on 15 UTE-MRI datasets, of which some examples are shown in Figure 10. Despite the fact that the vascular trees segmented from UTE-MRI are less dense than those obtained from CT data, the lobe segmentation results are visually consistent and can be further on exploited in future studies on regional ventilation measurements.

6. Conclusion

This paper develops an automated approach for lung lobes partitioning in ultra-short time echo (UTE) MRI pulmonary data exploiting the segmentation of the vascular network and its clustering in lobes. Vascular clustering is based on the inference of a PointNet++ model trained on CT data and on graph cuts removing eventual connections between the lobes. The results obtained show pertinent lung partitioning which opens the possibility of regional assessment of ventilation patterns in proton MRI spirometry.

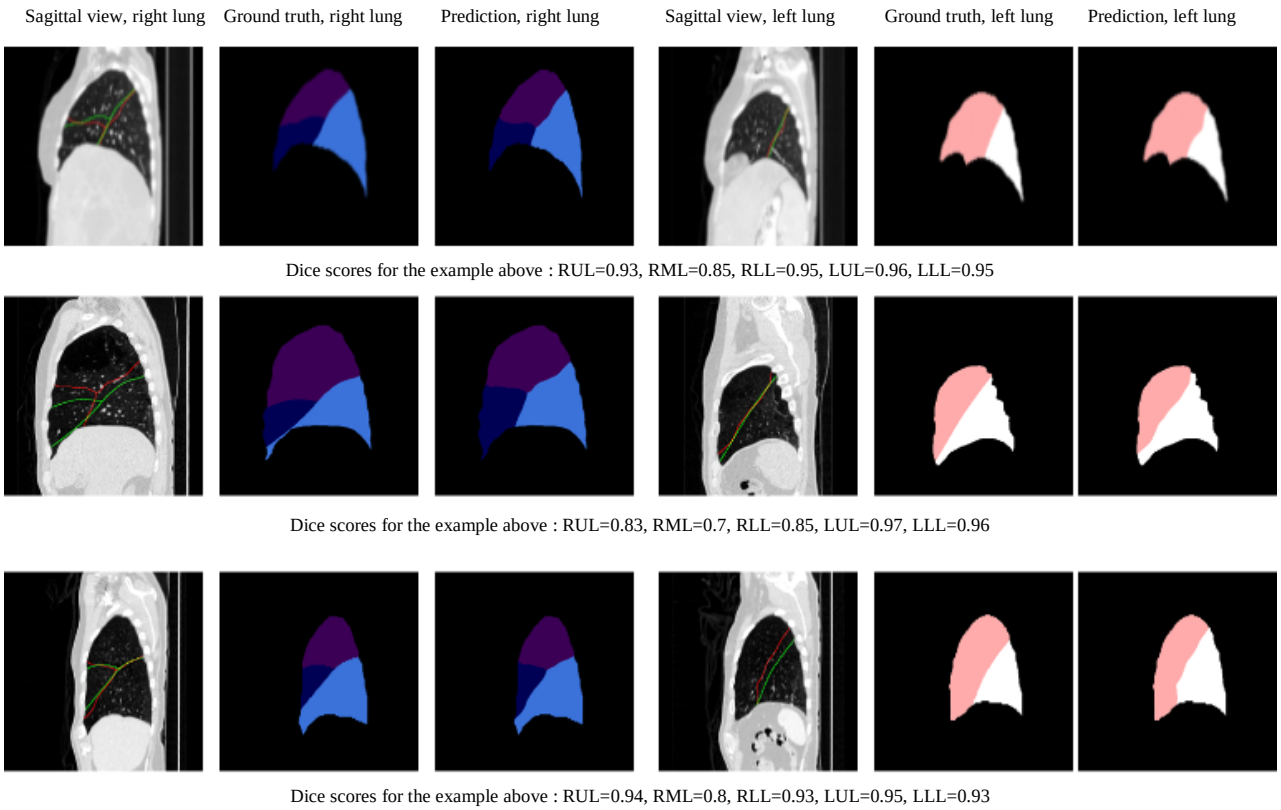

Figure 9. Sagittal views analysis of right and left lungs: a detailed comparison of ground truth and predicted masks with Dice score evaluation and fissure line annotations, featuring two columns for right and left lung representations. Within these images, fissure lines are distinctly marked, with red lines indicating predicted fissure locations and green lines representing the ground truth fissure.

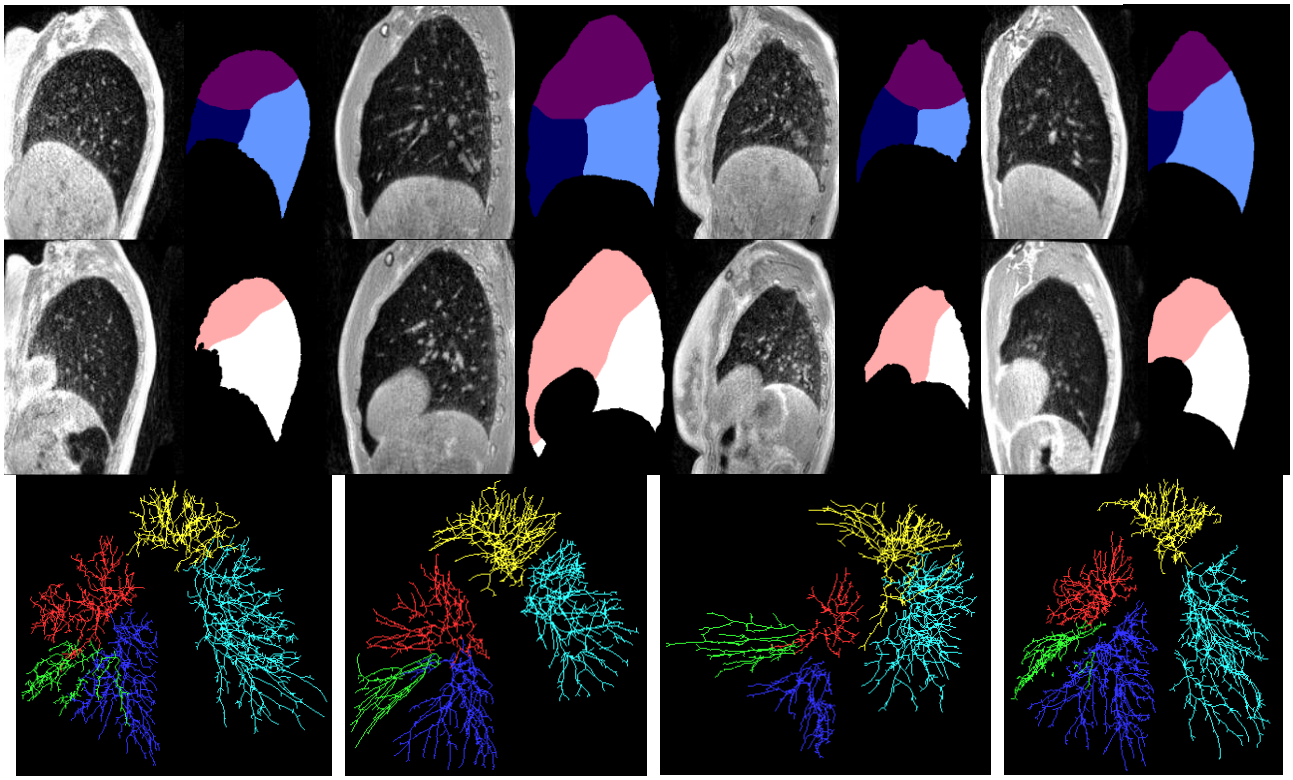

Figure 10. Sagittal views of lung lobe partitioning for UTE-MRI acquisitions in four patients (supine and prone positions) together with clustered vessel axis (latero-basal views; RUL – red, RML – green, RLL – blue, LUL – yellow, LLL - cyan).

Acknowledgement

The study was funded by the COVALung project (Fondation du Souffle, France), European Union Horizon Europe Research and Innovation Program under Grant Agreement N° 101099934 (VLFSpiro3D project), and ANR MLQ-CT.

References

1. Vogel-Claussen J, Kaireit TF, Voskrebenzev A, Klimeš F, Glandorf J, Behrendt L, Gutberlet M, Korz C, Speth M, Welte T, Wacker F, Gottlieb J.(2023). Phase-resolved functional lung (PREFUL) MRI–derived ventilation and perfusion parameters predict future lung transplant loss. Radiology.307(4). doi: 10.1148/radiol.22195
2. Capaldi, D. P., Guo, F., Xing, L., & Parraga, G. (2021). Pulmonary ventilation maps generated with free-breathing proton MRI and a deep convolutional neural network. Radiology, 298(2), 427-438. doi: 10.1148/radiol.2020202861.
3. Woods JC, Wild JM, Wielpütz MO, Clancy JP, Hatabu H, Kauczor HU, van Beek EJR, Altes TA.. (2020). Current state of the art MRI for the longitudinal assessment of cystic fibrosis. Journal of Magnetic Resonance Imaging, 52(5), 1306-1320. doi: 10.1002/jmri.27030
4. Tang, H., C. Zhang, and X.J.a.p.a. Xie, Automatic Pulmonary Lobe Segmentation Using Deep Learning. (2019). (https://arxiv.org/abs/1903.09879)
5. Park J, Yun J, Kim N, Park B, Cho Y, Park HJ, Song M, Lee M, Seo JB. Fully Automated Lung Lobe Segmentation in Volumetric Chest CT with 3D U-Net: Validation with Intra- and Extra-Datasets. J Digit Imaging, 2020 Feb. doi: 10.1007/s10278-019-00223-1
6. Hoileong Lee and Tahreema Matin and Fergus Gleeson and Vicente Grau. (2019). Efficient 3D Fully Convolutional Networks for Pulmonary Lobe Segmentation in CT Images. (https://arxiv.org/abs/1909.07474)

7. Gerard, S.E. and J.M. Reinhardt. Pulmonary Lobe Segmentation Using A Sequence of Convolutional Neural Networks For Marginal Learning. in 2019 IEEE 16th International Symposium on Biomedical Imaging (ISBI 2019). 2019. IEEE. doi: 10.1109/ISBI.2019.8759212.
8. Wang, W., et al. (2019). Automated Segmentation of Pulmonary Lobes using Coordination-Guided Deep Neural Networks. 2019 IEEE 16th International Symposium on Biomedical Imaging. (https://arxiv.org/pdf/1904.09106.pdf)
9. F. T. Ferreira, P. Sousa, A. Galdran, M. R. Sousa and A. Campilho. End-to-end supervised lung lobe segmentation. in 2018 International Joint Conference on Neural Networks (IJCNN). 2018. IEEE. pp. 1-8, doi: 10.1109/IJCNN.2018.8489677.
10. Kevin George, Adam P. Harrison, Dakai Jin, Ziyue Xu & Daniel J. Mollura. (2017). Pathological pulmonary lobe segmentation from CT images using progressive holistically nested neural networks and random walker, in Deep Learning in Medical Image Analysis and Multimodal Learning for Clinical Decision Support. 2017, Springer. p. 195-203. https://doi.org/10.1007/978-3-319-67558-9_23
11. Charles R. Qi and Li Yi and Hao Su and Leonidas J. Guibas. (2017). PointNet++: Deep Hierarchical Feature Learning on Point Sets in a Metric Space. https://doi.org/10.48550/arXiv.1706.02413
12. Kim Y-W, Tarando SR, Brillet P-Y and Fetita C. (2019). Image biomarkers for quantitative analysis of idiopathic interstitial pneumonia. SPIE Medical Imaging 2019: Computer-Aided Diagnosis, pp.10950-44, ⟨10.1117/12.2511847⟩
13. Fetita et al., "Robust lung identification in MSCT via controlled flooding and shape constraints: dealing with anatomical and pathological specificity," in SPIE Medical Imaging 2016: Biomedical Applications in Molecular, Structural, and Functional Imaging vol. 9788, 2016.
14. A.F.Kouvahé, C.Fetita, "A Generic Approach for Efficient Detection of Vascular Structures", IRBM 2020, https://doi.org/10.1016/j.irbm.2020.06.011
15. Fetita C. *et al*, Multiparameter analysis of vascular remodeling in post-acute sequelae of COVID-19, Proceedings Volume 12033, Medical Imaging 2022: Computer-Aided Diagnosis; 120330A (2022) https://doi.org/10.1117/12.2611461
16. Fetita C, et al, "Airway shape assessment with visual feed-back in asthma and obstructive diseases" in Medical Imaging 2010: Visualization, Image-Guided Procedures, and Modeling, Proceedings of SPIE Vol. 7625, p. 76251E:1-12.
17. Fetita C., *et al*, "A morphological-aggregative approach for 3D segmentation of pulmonary airways from generic MSCT acquisitions". *Proc. of Second International Workshop on Pulmonary Image Analysis* - MICCAI'09, 215-226 (2009).
18. Catalin Fetita, Pierre-Yves Brillet, Christopher Brightling, Philippe Grenier, "Grading remodeling severity in asthma based on airway wall thickening index and bronchoarterial ratio measured with MSCT", Proceedings Volume 9415, Medical Imaging 2015: Image-Guided Procedures, Robotic Interventions, and Modeling; 941515 (2015) https://doi.org/10.1117/12.2081589